Sung et al. Journal of Biomedical Science (2022) 29:52
https://doi.org/10.1186/s12929-022-00832-z

MOST 科技部 Ministry of Science and Technology
The cost of publication in Journal of Biomedical Science is borne by the Ministry of Science and Technology, Taiwan.
Journal of Biomedical Science

RESEARCH

Open Access

CLEC5A and TLR2 are critical in SARS-CoV-2-induced NET formation and lung inflammation

Pei-Shan Sung[1], Shao-Ping Yang[1], Yu-Chun Peng[1], Cheng-Pu Sun[2], Mi-Hwa Tao[2] and Shie-Liang Hsieh[1,3,4,5*]

Abstract

Background: Coronavirus-induced disease 19 (COVID-19) infects more than three hundred and sixty million patients worldwide, and people with severe symptoms frequently die of acute respiratory distress syndrome (ARDS). Recent studies indicated that excessive neutrophil extracellular traps (NETs) contributed to immunothrombosis, thereby leading to extensive intravascular coagulopathy and multiple organ dysfunction. Thus, understanding the mechanism of severe acute respiratory syndrome coronavirus 2 (SARS-CoV-2)-induced NET formation would be helpful to reduce thrombosis and prevent ARDS in severe acute respiratory syndrome coronavirus 2 (SARS-CoV-2) infection.

Methods: We incubated SARS-CoV-2 with neutrophils in the presence or absence of platelets to observe NET formation. We further isolated extracellular vesicles from COVID-19 patients' sera (COVID-19-EVs) to examine their ability to induce NET formation.

Results: We demonstrated that antagonistic mAbs against anti-CLEC5A mAb and anti-TLR2 mAb can inhibit COVID-19-EVs-induced NET formation, and generated *clec5a*$^{-/-}$/*tlr2*$^{-/-}$ mice to confirm the critical roles of CLEC5A and TLR2 in SARS-CoV-2-induced lung inflammation in vivo. We found that virus-free extracellular COVID-19 EVs induced robust NET formation via Syk-coupled C-type lectin member 5A (CLEC5A) and TLR2. Blockade of CLEC5A inhibited COVID-19 EVs-induced NETosis, and simultaneous blockade of CLEC5A and TLR2 further suppressed SARS-CoV-2-induced NETosis in vitro. Moreover, thromboinflammation was attenuated dramatically in *clec5a*$^{-/-}$/*tlr2*$^{-/-}$ mice.

Conclusions: This study demonstrates that SARS-CoV-2-activated platelets produce EVs to enhance thromboinflammation via CLEC5A and TLR2, and highlight the importance of CLEC5A and TLR2 as therapeutic targets to reduce the risk of ARDS in COVID-19 patients.

Keywords: Platelets, COVID-19, Neutrophil extracellular traps, CLEC2, CLEC5A, TLR2, Immunothrombosis, SARS-CoV-2, Acute respiratory distress syndrome, Spike protein

Introduction

SARS-CoV-2 is the etiological agent of the COVID-19 [1, 2], and has claimed more than 5.62 million lives worldwide. One of the clinical features of severe SARS-CoV-2 infection is extensive infiltration of neutrophils and macrophages in lung, and COVID-19 patients suffer from ARDS caused by extensive lung inflammation, tissue injury, and fibrosis [3]. In addition, pulmonary embolism [4, 5], microangiopathy, cerebral infarction, [6] and visceral organ thrombo-emboli are frequently observed in post-mortem autopsy of COVID-19 patients [7, 8].

Thrombotic complication is a major cause of morbidity and mortality in patients with COVID-19 [9]. Even though the pathogenesis of thrombo-emboli formation

*Correspondence: slhsieh@gate.sinica.edu.tw

[1] Genomics Research Center, Academia Sinica, 128 Academia Road, Sec. 2, Nankang, Taipei 115, Taiwan
Full list of author information is available at the end of the article

in COVID-19 patients is still unclear, recent studies indicate that excessive NET production is associated with thrombo-emboli formation in human diseases. It has been reported that elevated levels of cell-free DNA, myeloperoxidase, and citrullinated histone H3 are noted in the sera of COVID-19 patients, and higher levels of NET formation correlated with disease severity [10, 11]. Thus, targeting excessive NET formation is speculated to reduce pulmonary inflammation and thrombosis in COVID-19 patients [12].

Because platelets are hyperactivated in critically ill COVID-19 patients [13, 14], and platelets-neutrophil interactions play critical roles in endothelial damage and immunothrombosis of COVID-19 patients [15–17], we are interested to understand the molecular mechanism of platelets-mediated enhancement of NET formation and pulmonary inflammation in SARS-CoV-2 infection. Recently, SARS-CoV-2 was shown to activate platelets to enhance thrombosis in vivo [18], and serum levels of platelet-derived EVs (PLT-EVs) strongly associated with severity of SARS-CoV-2 infection [19]. Moreover, sera from COVID-19 patients trigger NET formation in neutrophils isolated from healthy donors [20]. These observations suggest that SARS-CoV-2 may activate platelets to release EVs, thereby induce NET formation and immunothrombosis in COVID-19 patients.

We have demonstrated that dengue virus (DV) [21–24] and microbes [25] bind and activate CLEC5A and TLR2 to release proinflammatory cytokines and promote NET formation. Moreover, DV activates Syk-coupled C-type lectin member 2 (CLEC2) in platelets to release EVs to enhance DV-induced NET formation and macrophage activation via CLEC5A and TLR2 [26, 27]. Recently, SARS-CoV-2 spike protein was reported to induce NETosis in Syk-dependent manner [28], suggesting that C-type lectins might play important roles in SARS-CoV-2-induced NET formation. Moreover, TLR2 was shown to sense SARS-CoV-2 membrane protein to activate NF-kB in monocyte and macrophages [29, 30]. Because CLEC5A and TLR2 are associated and co-activated by platelet-derived EVs (PLT-EVs) [26], we asked whether CLEC5A and TLR2 also contributed to SARS-CoV-2-induced immunothrombosis.

Here we report that COVID-19 EVs express abundant markers of activated platelets, and induce NET formation via CLEC5A and TLR2. Simultaneous blockade of CLEC5A and TLR2 inhibited SARS-CoV-2-induced NET formation in vitro, and thromboinflammation and fibrosis were dramatically attenuated in *clec5a*$^{-/-}$/*tlr2*$^{-/-}$ mice. These observations suggest that EVs from virus-activated platelets play as endogenous danger signals to trigger NETs and inflammatory reactions via CLEC5A and TLR2, and blockade of CLEC5A and TLR2 may become a promising strategy to attenuate SARS-CoV-2-induced thrombus and coagulopathy in COVID-19 patients in the future.

Materials and methods

Reagents and antibodies

All culture media and buffers were purchased from Gibco. The source of anti-hCLEC5A mAb (clone 3E12A2) and anti-hTLR2 mAb (# MAB2616, R and D system) were as previously described [18]. Antibodies for immunofluorescence staining are as followings: rabbit anti-citrullinated histone H3 (#NB100-57135; Novus), goat anti-human/mouse myeloperoxidase polyclonal antibody (# AF3667, R&D system). Antibodies for immunohistochemical (IHC) staining are: rabbit anti-citrullinated histone H3 (#NB100-57135; Novus), goat anti-human/mouse myeloperoxidase polyclonal antibody (#AF3667, R&D system), anti-CD11b antibody (#ab13357, Abcam), anti-CD64 antibody (#MA5-29704, Invitrogen), anti-Siglec-F antibody (#PA5-11675, Invitrogen), anti-F4/80 antibody (#ab74383, Abcam), anti-CCR2 antibody (#NBP-35334, Novus Biologicals), anti-Ly6C antibody (#SC-23080, Santa Cruz). Secondary antibodies: donkey anti-mouse IgG (H + L) Alexa 488-conjugated antibody (#715-545-151, Jackson ImmunoResearch), donkey anti-goat IgG (H + L) Alexa 647-conjugated antibody (#705-605-147, Jackson ImmunoResearch), donkey anti-Human IgG (H + L) HRP-conjugated antibody (#709-035-149, Jackson ImmunoResearch), HRP-conjugated donkey anti-rabbit IgG (H + L) (#711-035-152, Jackson ImmunoResearch), HRP-conjugated donkey anti-goat IgG (H + L) (#SC-2020, Santa Cruz), HRP-conjugated donkey anti-mouse IgG (H + L) (#715-035-150, Jackson ImmunoResearch).

Isolation of human primary neutrophils and platelets

Blood was drawn from healthy donors (unvaccinated with SARS-CoV-2 vaccine) into an anticoagulant ACD-containing syringe (ACD: blood ratio = 1:6, v/v), platelet-rich plasma was collected by centrifuge at 230 × *g* for 15 min. Pellet of platelets was harvested by centrifugation at 1000 × *g* for 10 min, then suspended in Tyrode's buffer. For human neutrophils, whole blood was laid on the Ficoll-Paque (GE Healthcare, 45-001-748) and centrifuged at 500 × *g* for 15 min to get red blood cells (RBCs)-granulocytes-rich layer. After RBC lysis, neutrophils were washed and suspended in RPMI containing 10% serum from unvaccinated blood type A/B healthy donors. The protocol was approved by the Human Subject Research Ethics, Academia Sinica (AS-IRB-BM-20025).

Isolation of mouse primary neutrophils and platelets

Platelets-rich plasma from murine peripheral blood was collected into ACD-containing Eppendorf and centrifugated at 230 × *g* for 4 min. Platelets were washed once and harvested by centrifugation at 1000 × *g* for 4 min, pellet was suspended in Tyrode's buffer. For neutrophil isolation, bone marrow was collected and incubated with RBC lysis buffer. Bone marrow cells were suspended in a 45% Percoll solution, then laid on 52%, 63%, and 81% Percoll, and were further centrifugated at 1000 × *g* for 30 min. Neutrophils were harvested from layer 3 of the Percoll gradient, followed by washing with HBSS twice before being suspended in RPMI containing 10% FBS.

SARS-CoV-2 propagation

SARS-CoV-2 Taiwan/4/2020 was propagated in Vero E6 cells. Viral titer was determined by observation of the cytopathic effect (CPE) in Vero cells. This strain was used in all of the experiments.

Production and purification of pseudotyped lentivirus

The pseudotyped lentivirus carrying the SARS-CoV-2 spike protein was generated as described previously [31]. In brief, HEK-293 T cells were transiently transfected with pLAS2w.Fluc.Ppuro, pcDNA3.1-2019-nCoV-S, and pCMV-ΔR8.91 using TransITR-LT1 transfection reagent (Mirus). Cell debris was removed by centrifugation at 4000 × *g* for 10 min, followed by passing the supernatant through a 0.45 μm syringe filter (Pall Corporation). For pseudotyped virus purification and concentration, supernatant was mixed with 0.2 × volume of 50% PEG 8,000 (Sigma) and incubated at 4 °C for 2 h. The pseudotyped lentivirus was then recovered by centrifugation at 5000 × *g* for 2 h, and resuspended in sterilized phosphate-buffered saline, aliquoted, and stored at − 80 °C.

Mouse model for SARS-CoV-2 infection

Virus preparation and inoculation of SARS-CoV-2 into C57BL/6 and *clec5a*$^{-/-}$/*tlr2*$^{-/-}$ mice were as described [32]. In brief, mice were intranasally injected with 3×10^{11} vg of AAV6/hACE2 in 50 μl saline before 14 days of SARS-CoV-2 inoculation, then C57BL/6 and *clec5a*$^{-/-}$/*tlr2*$^{-/-}$ mice ($N = 3$ of each group) were intranasally changed with 1×10^5 TCID50 of SARS-CoV-2 in a volume of 100 μl. Lung tissue was collected at 3 days and 5 days post-infection for further analysis. All the animal experiments followed the protocol approved by the Institutional Animal Care and Use Committee (IACUC) at AS core (protocol ID 20-10-1521).

Collection of tissues for RNA isolation

Mice were sacrificed at 3 days and 5 days post-infection. For RNA isolation, lung was dug into TRizol-containing MagNA Lyser Green Beads (Roche) for tissue homogenization and further isolated RNA using TriRNA Pure Kit (Geneaid) according to the manufacturer's instruction. cDNA was synthesized using the RevertAid First Strand cDNA Synthesis Kit and the real-time PCR was performed as followed conditions: 95 °C for 5 min, followed by 30 cycles of 15 s at 95 °C, 30 s at 58 °C, and 30 s at 72 °C. The primer sequences were listed in Additional file 2: Table S1. Data were shown as fold change compared to mock after normalized to GAPDH.

Immunohistochemistry (IHC)

Lung tissue was fixed in 10% paraformaldehyde for 48 h and embedded in paraffin subsequently. Tissue sections were deparaffined and rehydrated before H&E stain and multiple-color fluorescent staining using Opal 7-Color IHC Kits (Akoya bioscience). Samples were incubated with primary antibody (1:50) at 4 °C overnight, followed by incubation with secondary antibody (1:100) at room temperature for 1 h. The Opal fluorescent dye was applied according to the vendor's instructions. Images were captured with a Leica confocal microscope with white light laser system (TCS SP8X-FALCON) and exported using the Leica Application Suite X software. The NET/thrombosis quantitation and cell population analysis by MetaMorph™ image software.

Collagen deposition

Lung sections were de-paraffined and re-hydrated before being stained with Picro Sirius Red Stain Kit (#ab150681, Abcam), and images were captured by a light microscope with polarized light (Nikon). Quantification of collagen was performed by MetaMorph™, and the level of collagen deposition was presented as area (μm^2) of collagen under 20× and 40× magnification, repectively. For Masson's trichrome stain, tissue sections were stained with Trichrome Stain (Masson) Kit (Sigma, # HT15-1KT), the level of pulmonary fibrosis was evaluated by the modified Ascroft scale as previously described [33].

Isolation of extracellular vesicles (EVs)

Plasma from healthy donors and COVID-19 patients with severe pneumonia were centrifugated at 3500 × *g* for 15 min to remove cells and debris. Supernatants were further centrifuged at 100,000 × *g* for 1.5 h at 4 °C. Pellets were washed with saline and centrifuged at 100,000 × *g* for 1.5 h at 4 °C, followed by resuspension in 1 ml of saline. The protein concentration of EVs was determined by DC protein assay (Bio-Rad) according to the manufacturer's instruction.

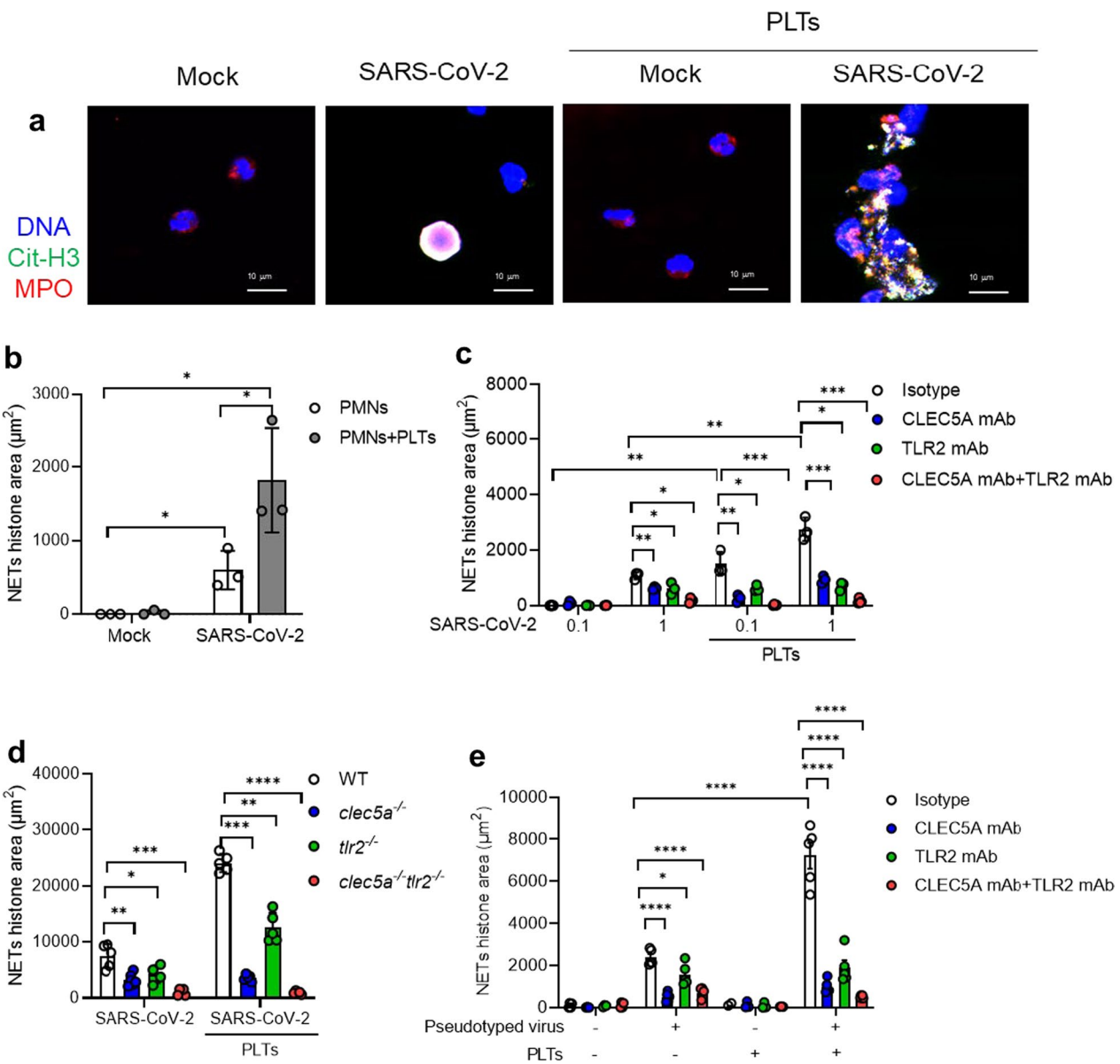

Fig. 1 CLEC5A and TLR2 are responsible for SARS-CoV-2-induced NET formation. **a**, **b** Neutrophils (4×10^5/ml) from healthy donors were incubated with SARS-CoV-2 (MOI = 1) with or without autologous platelets (4×10^6/ml) for 5 h at 37 °C. The scale bar is 10 μm. The detailed structure of SARS-CoV-2-induced NET formation was observed under a confocal microscope (Leica). NET formation was visualized by fluorescent staining of DNA (blue), histone (green), and MPO (red) **a** NETs level was measured by MetaMorph software and presented as Cit-H3 area (μm^2) (**b**). **c** Human neutrophils (4×10^5/ml) were pretreated with anti-hCLEC5A mAb (3E12A2, 10 μg/ml), anti-TLR2 mAb (# MAB2616, 10 μg/ml), or combination of both antibodies for 30 min at room temperature, followed by incubation with SARS-CoV-2 (MOI = 0.1 and 1) in the presence or absence of platelets (4×10^6/ml) for 5 h and 20 h. The level of NET formation was determined by histone area (μm^2). **d** Neutrophils (4×10^5/ml) from WT, *clec5a*$^{-/-}$, *tlr2*$^{-/-}$, and *clec5a*$^{-/-}$*tlr2*$^{-/-}$ mice were incubated with SARS-CoV-2 (MOI = 1) in the presence or absence of WT platelets (4×10^6/ml) for 5 h at 37 °C. **e** Human neutrophils were pre-treated with anti-hCLEC5A mAb (3E12A2, 100 μg/ml), anti-TLR2 mAb (# MAB2616, 100 μg/ml), or combination of both antibodies for 30 min at room temperature, followed by incubation with SARS-CoV-2 spike pseudotyped virus (MOI = 0.1) in the presence or absence of autologous platelets (4×10^6/ml) for 3 h. Data are mean ± SEM and repeats of 3 to 5 independent experiments. *$p < 0.05$, **$p < 0.01$, ***$p < 0.001$, ****$p < 0.0001$ (Student's *t*-test).

Surface markers measurement by flow cytometry

The EVs from healthy control (HC, $n = 3$) and COVID-19 patient ($n = 10$) plasma were suspended in saline, then stained with capture beads and detection reagents according to the manufacturer's instruction. The surface markers level was measured by flow cytometry

FACSVerse™ and presented as mean fluoresce intensity (MFI). Statistical analysis was calculated with an unpaired and nonparametric Student's *t*-test with Mann–Whitney test. ns: no significant difference, $^{*}p < 0.05$, $^{**}p < 0.01$.

Induction of neutrophil extracellular traps (NETs)

Human neutrophils (4×10^5/ml) were seeded on poly-L-lysine-coated 12 mm coverslip in 24 well and simultaneously incubated with SARS-CoV-2 (MOI = 0.1 or 1) in presence of autologous platelets (4×10^6/ml) for 5 or 20 h at 37 °C. For SARS-CoV-2-spike pseudotyped virus stimulation, human neutrophils (4×10^5/ml) were incubated with SARS-CoV-2-spike pseudotyped virus (MOI = 0.25) and co-incubated with autologous platelets (4×10^6/ml) for 3 h at 37 °C. For blocking assay, neutrophils were pre-incubated with isotype (10 μg/ml), anti-CLEC5A mAb (10 μg/ml, clone 3E12A2), anti-TLR2 mAb (10 μg/ml, R&D system), or a mixture of anti-CLEC5A mAb and anti-TLR2 mAb for 30 min at room temperature before incubation with SARS-CoV-2. For EVs stimulation assay, neutrophil was incubated with EVs from the plasma of healthy controls (HC-EVs) or COVID-19 EVs for 3 h at 37 °C.

Visualization and quantification of NET structure

Cells were immersed in fixation buffer (containing 4% paraformaldehyde) overnight, followed by permeabilization using 0.5% Triton X100 in PBS, then incubated with anti-MPO antibody (1:100), anti-citrullinated histone antibody (1:100), and Hoechst 33342 (1:100,000). The level of NETs was calculated using the histone image captured by a Leica confocal microscope with white light laser system (TCS SP8 X-FALCON), and analyzed by MetaMorph™ software.

Mass spectrometry analysis and ingenuity pathways analysis (IPA)

Mass spectrometry analysis was performed in the Mass Spectrometry Core Facility located in the Genomic Research Center, Academia Sinica. In brief, EVs samples were lysed by RIPA solution containing phosphatase and protease inhibitors. Before the mass spectrometry analysis, samples were washed in PBS, followed by trypsin digestion before subjected to LTQ Orbitrap XL mass spectrometer (Thermo Fisher Scientific Inc.). Data were further analyzed by the Ingenuity Pathways Analysis (IPA) software. The significance of *p*-value was calculated by the right-tailed Fisher's Exact Test and shown as -log (*p*-values).

Statistical analysis

All the numbers of samples or mice were described in the figure legend, and the statistical significance was calculated using GraphPad Prism (version 9.0) software (GraphPad Software Inc., San Diego, CA, USA). Data were presented as mean ± SEM and the statistical significance was measured using an unpaired and nonparametric Student's *t*-test with Mann–Whitney test. In all of the experiments, $^{*}p < 0.05$, $^{**}p < 0.01$, $^{***}p < 0.001$, $^{****}p < 0.0001$.

Results

SARS-CoV-2 induces robust NET formation in the presence of platelets

To understand the role of platelet in SARS-CoV-2-induced NET formation, SARS-CoV-2 were incubated with human neutrophils in the presence or absence of autologous platelets. At 5 h post-incubation with SARS-CoV-2 (MOI = 1) (2nd panel from left, Fig. 1a), SARS-CoV-2 alone induced colocalization of citrullinated histone (Cit-H3), chromosomal DNA, and myeloperoxidase (MPO) within neutrophils. In contrast, robust aggregated NETs were observed in the presence of platelets (4th panel from the left, Fig. 1a), which is distinct from the thread-like NET structure induced by DV/platelets [26]. The detail of NET structure was presented as separated panels in Additional file 1: Fig. S1 & S2, and the level of NETs was measured by Cit-H3 area (μm^2) (Fig. 1b). These observations demonstrated the critical role of platelets in SARS-CoV-2-induced NET formation.

(See figure on next page.)

Fig. 2 COVID-19 EVs are derived from activated platelets and induce NET formation via CLEC5A. **a** EVs from healthy controls (HCs-EVs, $n = 2$) and COVID-19 patients (COVID19-EVs, $n = 5$) were harvested by ultracentrifugation, then lysed in RIPA solution before subjected to mass spectrometry analysis. Proteins expressed in COVID-19 EVs, but not in HCs EVs, were further analyzed using the QIAGEN Ingenuity Pathway Analysis (QIAGEN IPA) software. Proteins which were expressed in all the COVID19-EVs were displayed. **b**, **c** HCs-EVs ($n = 3$) and COVID19-EVs ($n = 10$) were analyzed by flow cytometry, and markers highly activated in COVID-19 platelets were expressed as a heat map (**b**) or by mean fluorescence intensity (**c**). **d** Neutrophils were pre-incubated with anti-CLEC5A mAb (3E12A2, 10 μg/ml), anti-TLR2 mAb (# MAB2616, 10 μg/ml), or both anti-CLEC5A mAb (3E12A2, 10 μg/ml) and anti-TLR2 mAb (# MAB2616, 10 μg/ml), for 30 min at room temperature, followed by incubation with EVs (1 μg/ml) from COVID-19 patients ($n = 6$) at 37 °C for 3 h. Data are mean ± sd and repeats of at least three independent experiments. *n.s.*: no significant differences, $^{*}p < 0.05$, $^{**}p < 0.01$, $^{***}p < 0.001$, $^{****}p < 0.0001$ (Student's *t*-test). N.D: not detectable

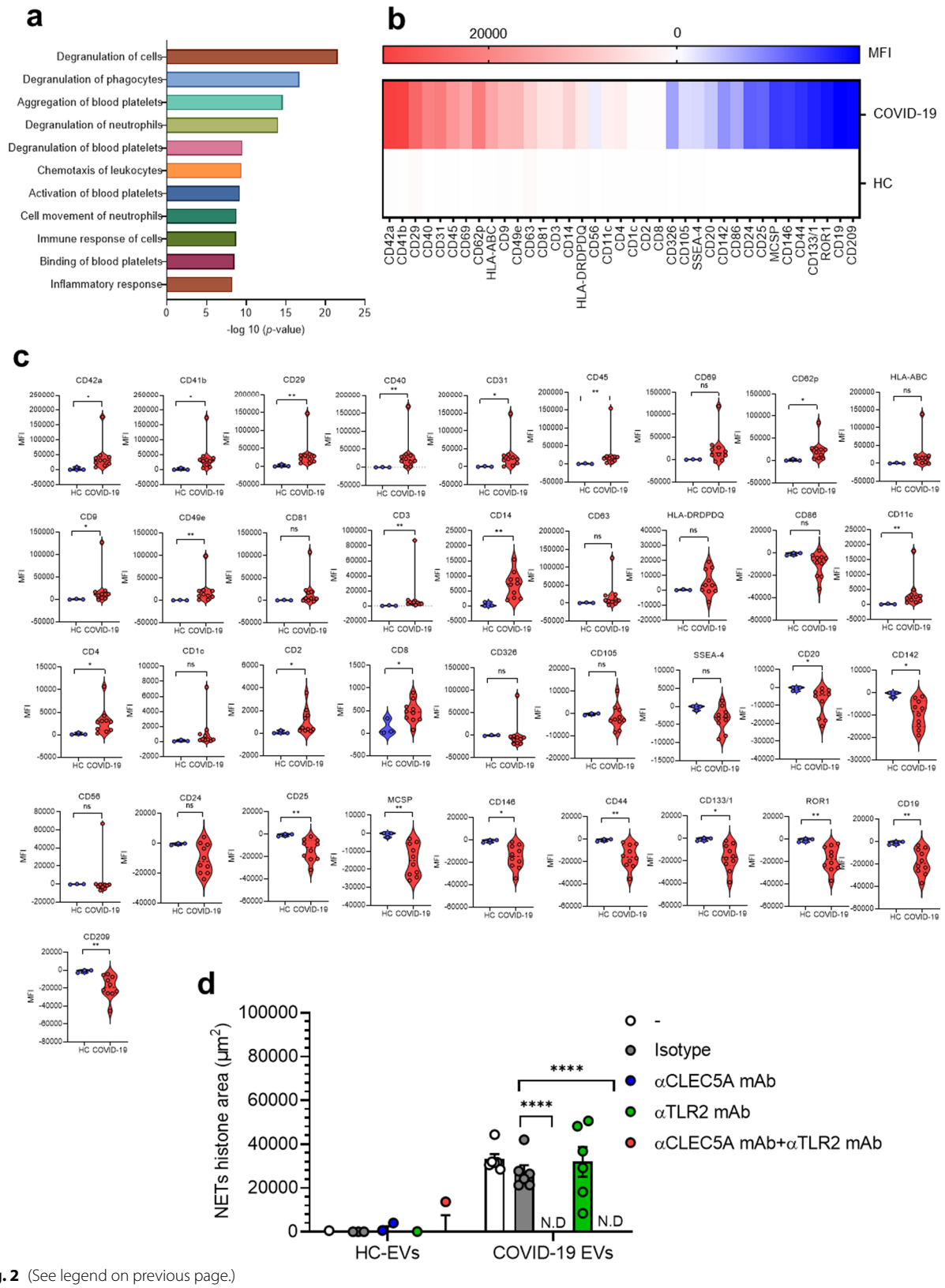

Fig. 2 (See legend on previous page.)

Table 1 Proteins expressed in COVID19-EVs

Diseases or functions annotation	Molecules	Number of molecules	-log 10 (*p*-value)
Degranulation of cells	ACTN4, ACTR2, ADAM10, ALAD, ANPEP, APP, CALM1, CCT8, CD226, CD47, CD84, CD9, CNN2, COTL1, CYB5R3, CYFIP1, DBNL, DDOST, EEF1A1, ENDOD1, GDI2, GPI, HPSE, HSP90AB1, IQGAP2, LYN, MMRN1, NCKAP1L, PEBP1, PF4, PGRMC1, PTPN6, RAB10, RAB27B, RAB5C, RALB, SELP, SERPINB1, STX11, SYTL4, TGFB1	41	21.55752
Degranulation of phagocytes	ACTR2, ADAM10, ALAD, ANPEP, APP, CCT8, CD226, CD47, CD84, CD9, CNN2, COTL1, CYB5R3, CYFIP1, DBNL, DDOST, EEF1A1, GDI2, GPI, HPSE, HSP90AB1, IQGAP2, LYN, NCKAP1L, PEBP1, PF4, PGRMC1, PTPN6, RAB10, RAB5C, SERPINB1, STX11	32	16.71444
Aggregation of blood platelets	ALOX12, ANXA7, APP, CD47, CD9, CLEC2, GNAQ, GNAZ, GP5, LYN, MPIG6B, MYLK, P4HB, PDIA4, PTPN6, RAB27B, SELP, TGFB1, TREML1, VASP	20	14.64782
Degranulation of neutrophils	ACTR2, ADAM10, ALAD, ANPEP, CCT8, CD47, CNN2, COTL1, CYB5R3, CYFIP1, DBNL, DDOST, EEF1A1, GDI2, GPI, HPSE, HSP90AB1, IQGAP2, NCKAP1L, PF4, PGRMC1, PTPN6, RAB10, RAB5C, SERPINB1, STX11	26	14.03905
Degranulation of blood platelets	ACTN4, APP, CALM1 (includes others), CD9, ENDOD1, LYN, MMRN1, PF4, RAB27B, SELP, SYTL4, TGFB1	12	9.527244
Chemotaxis of leukocytes	ADAM10, APP, CD47, CD9, DNM1L, GNAZ, HPSE, HSPD1, JAM3, LYN, MYLK, NCKAP1L, PF4, PLEC, PPIB, PRKCB, PTPN6, SELP, SERPINB1, TGFB1, TXN	21	9.425969
Activation of blood platelets	CLEC2, GNAQ, GNB1, GP1BB, GP5, LYN, MPIG6B, PF4, PRKCB, PTPN6, SELP, TREML1, VASP	13	9.191789
Cell movement of neutrophils	ADAM10, APP, CD47, CNN2, DNM1L, HSPB1, JAM3, LYN, MYLK, NCKAP1L, PF4, PRKCB, PTPN6, RTN4, SELP, SERPINB1, TGFB1, TXN, VASP	19	8.793174
Immune response of cells	ACTR2, ANPEP, ANXA11, APP, CALR, CD226, CD47, CLIC4, CNN2, CORO1C, CYFIP1, DNM1L, EHD1, HSP90B1, HSPB1, IGHA2, KIF2A, LTBP1, LYN, NCKAP1L, PF4, PRKCB, PTPN6, RAB11A, RALB, TGFB1, VASP	27	8.742321
Binding of blood platelets	APP, CD226, CD84, CLEC2, FYB1, GP5, JAM3, PPIB, SELP, VASP	10	8.542118
Inflammatory response	ADAM10, APP, CD226, CD47, CD84, CD9, DNM1L, FKBP1A, GNAZ, GPX1, HPSE, HSPB1, HSPD1, JAM3, LTBP1, LYN, MAOB, MYLK, NCKAP1L, PF4, PLEC, PPIB, PRDX5, PRKCB, PTPN6, RALB, SELP, SERPINB1, TGFB1, TUBA1C, TXN	31	8.271646

The mass spectrum analysis was performed using the LTQ Orbitrap XL mass spectrometer (Thermo Fisher Scientific Inc.) and the proteomics data were further analyzed by Ingenuity Pathways Analysis (IPA) software. The unique proteins present in EVs form COVID-19 patients (COVID19-EVs) were listed in the table according to the result of IPA analysis

CLEC5A and TLR2 are critical in NET formation caused by SARS-CoV-2

Our previous works demonstrated that CLEC5A and TLR2 were critical for virus and microbes-induced NET formation [26, 27], thus we further asked whether CLEC5A and TLR2 contributed to SARS-CoV-2-induced NETosis. We found that SARS-CoV-2 alone induced NET formation in a higher dose (MOI = 1) at 5 h post-incubation (left, Fig. 1c). In the presence of platelets, SARS-CoV-2-induced NET formation was further enhanced (right, Fig. 1c). While NET formation was partially inhibited by anti-CLEC5A mAb and anti-TLR2 mAb, simultaneous blockade of CLEC5A and TLR2 almost completely suppressed SARS-CoV-2-induced NET formation (Fig. 1c). This observation suggests that platelet is a potent enhancer in SARS-CoV-2-induced NET formation.

We further incubated SARS-CoV-2 and SARS-CoV-2 plus platelets (SARS-CoV-2/platelets) with wild-type (WT) and *clec5a*$^{-/-}$*tlr2*$^{-/-}$ neutrophils, respectively, in the absence (left, Fig. 1d) or presence of WT platelets (right, Fig. 1d). We found that SARS-CoV-2 and SARS-CoV-2/platelets-induced NET formation was partially attenuated in *clec5a*$^{-/-}$ neutrophils and *tlr2*$^{-/-}$ neutrophils, while NET formation was almost undetectable in *clec5a*$^{-/-}$*tlr2*$^{-/-}$ neutrophils. This observation further confirms the critical roles of CLEC5A and TLR2 in SARS-CoV-2 and SARS-CoV-2/platelets-induced NET formation.

We further asked whether SARS-CoV-2 spike protein contributed to platelet activation by incubating SARS-CoV-2 spike pseudotyped virus with neutrophils for NETosis assay. We found that platelets still enhanced SARS-CoV-2 spike pseudotyped virus-induced NET formation, though the enhancing effect was less obvious than SARS-CoV-2. Blockade of TLR2 (green bar) and CLEC5A (blue bar) partially inhibited NET formation, simultaneous blockade of CLEC5A and TLR2 abolished SARS-CoV-2 spike pseudotyped virus-induced NET formation dramatically (Fig. 1e). This observation suggests that SARS-CoV-2 spike protein co-activates CLEC5A and TLR2 to induce NET formation.

COVID-19 EVs induced NET formation via CLEC5A

As COVID-19 sera was reported to induce NET formation [20], and serum levels of platelet-derived EVs

Table 2 Change of surface markers in COVID19-EVs

Marker	Level in COVID-19 EVs (compared to HC-EVs)	*p*-value
CD42a	Upregulated	0.0140
CD41b	Upregulated	0.0140
CD29	Upregulated	0.0070
CD40	Upregulated	0.0070
CD31	Upregulated	0.0140
CD45	Upregulated	0.0070
CD69	No significantly different	0.1608
CD62p	Upregulated	0.0140
HLA-ABC	No significantly different	0.1119
CD9	Upregulated	0.0490
CD49e	Upregulated	0.0070
CD63	No significantly different	0.1608
CD81	No significantly different	0.3706
CD3	Upregulated	0.0070
CD14	Upregulated	0.0070
HLA-DRDPDQ	No significantly different	0.4685
CD56	No significantly different	0.1608
CD11c	Upregulated	0.0070
CD4	Upregulated	0.0140
CD1c	No significantly different	0.0769
CD2	Upregulated	0.0490
CD8	Upregulated	0.0490
CD326	No significantly different	0.0769
CD105	No significantly different	0.3706
SSEA-4	No significantly different	0.1608
CD20	Downregulated	0.0280
CD142	Downregulated	0.0140
CD86	No significantly different	0.0769
CD24	No significantly different	0.2168
CD25	Downregulated	0.0070
MCSP	Downregulated	0.0070
CD146	Downregulated	0.0140
CD44	Downregulated	0.0070
CD133/1	Downregulated	0.0140
ROR1	Downregulated	0.0070
CD19	Downregulated	0.0070
CD209	Downregulated	0.0070

The surface markers of EVs from healthy control (HC) and COVID-19 patients were measured using MACSPlex Exosome Kit (Miltenyi Biotec, #130-108-813) by flow cytometry FACverse. The expression level were presented as mean fluorescence intensity (MFI) and the statistical analysis was calculated using GraphPad Prism (version 9.0) software with an unpaired and nonparametric Student's *t*-test with Mann–Whitney test

(PLT-EVs) correlated with disease severity [19], we asked whether COVID-19 EVs induced NET formation was via CLEC5A and TLR2. Firstly, we compared the protein components of EVs isolated from serum samples of COVID-19 patients (COVID-19 EVs) and normal individuals (HC-EVs) by mass spectrometry, and data were analyzed by 'Ingenuity Pathway Analysis' (IPA, QIAGEN) software. We found that molecules involved in platelet degranulation (CD9, platelet factor 4 (PF4)), aggregation, and activation [CD9, CLEC1B (also known as CLEC2)] were upregulated dramatically in COVID-19 EVs, while none of these proteins were detectable in EVs from healthy donors (Fig. 2a). In addition to these upregulated molecules, proteins specifically expressed in COVID-19 EVs were listed in Table 1. We further confirmed the IPA results by flow cytometry analysis. We found that platelet activation markers (CD41a/b, CD62p), integrins (CD9, CD29, CD49e), adhesion molecules (CD31), and other activation marker (CD45, CD69) were upregulated (Fig. 2b, c). The change of surface marker expression with statistical significance is shown in Table 2. We then incubated neutrophils with HC-EVs and COVID-19 EVs, respectively, to compare their abilities to induce NET formation. While EVs from healthy control were unable to induce NET formation, COVID-19 EVs induced robust NET formation, which was blocked efficiently by anti-CLEC5A mAb, but not anti-TLR2 mAb (Fig. 2d). This observation suggests that COVID-19 EVs have potent activity to induce NET formation via CLEC5A.

CLEC5A and TLR2 are critical in SARS-CoV-2-induced thromboinflammation

We have used recombinant adeno-associated virus to introduce human ACE2 (hACE2) into wild type mice to establish a SARS-CoV-2 infection model system [32]. To evaluate the roles of CLEC5A and TLR2 in SARS-CoV-2-induced thromboinflammation, the AAV- hACE2 was introduced to wild-type littermates (WT) and *clec5a*$^{-/-}$*tlr2*$^{-/-}$ mice to address this question. In WT mice, SARS-CoV-2 upregulated the expression of IL-6, IFN-γ, CCL-2, and IP-10 dramatically (more than 10 folds, $p < 0.0001$), while TNF-α, IL-1β, I L-10, and chemokines (CXCL1, CXCL2, CXCL5) were also upregulated (more than 10 folds, $p < 0.0001$) (Fig. 3a). Compared to WT mice, the expression of proinflammatory cytokines and chemokines were downregulated in *clec5a*$^{-/-}$*tlr2*$^{-/-}$ mice. These observations demonstrated the critical role of CLEC5A and TLR2 in SARS-CoV-2-induced inflammatory reactions in lung tissues. We further detected NET formation in lung tissues after SARS-CoV-2 infection by examining the localization of DNA (blue), myeloperoxidase (green), citrullinated histone H3 (red), and platelet marker CD42b (yellow) (Fig. 3b and Additional file 1: Fig. S3). We found intense NET formation in lung tissue at day 3 and day 5 post-SARS-CoV-2 infection, while NET formation was almost undetectable in *clec5a*$^{-/-}$*tlr2*$^{-/-}$ mice (Fig. 3b and Additional file 1:Fig.

S3). The NET area and thrombi were further quantified by using anti-MPO antibody (Fig. 3c) and anti-CD42b antibody (Fig. 3d).

Moreover, severe infiltration of interstitial macrophages ($CD11b^+CD64^+F4/80^+$), monocyte-derived dendritic cell (DC)/macrophage (MΦ) ($CD11b^+CD64^+Ly6C^+$), and $Ly6C^+$ monocyte (gray column, Fig. 3e) into pulmonary area at day 3 post-SARS-CoV-2 infection were observed in WT mice. In contrast, cell infiltration was attenuated in *clec5a*$^{-/-}$*tlr2*$^{-/-}$ mice (red column, Fig. 3e). These observations indicated that CLEC5A and TLR2 are critical in SARS-CoV-2-induced thromboinflammation in vivo.

Attenuation of lung collagen deposition in mice deficient of CLEC5A and TLR2

In addition to thromboinflammation, SARS-CoV-2 infection resulted in lung injury and pulmonary fibrosis, including thickening of basement membranes and deposition of collagen [34]. Thus, we were interested to understand whether CLEC5A and TLR2 contributed to SARS-CoV-2-induced collagen deposition. At day 5 post-infection, severe thickening of alveolar cell wall and cell infiltration were noted in WT mice (upper middle, Fig. 4a), while these phenomena were attenuated in *clec5a*$^{-/-}$*tlr2*$^{-/-}$ mice after SARS-CoV-2 infection (upper right, Fig. 4a). We further examined the extent of collagen deposition by Masson's trichrome (lower panels, Fig. 4a) and Picro Sirius Red Staining (Fig. 4b). We observed yellow-orange birefringence (type I collagen thick fiber) and green birefringence (type III collagen, thin fiber) in lung tissues of WT mice after SARS-CoV-2 infection (middle panels, Fig. 4b). In contrast, collagen deposition was attenuated in *clec5a*$^{-/-}$*tlr2*$^{-/-}$ mice (right panels, Fig. 4b). The quantification of collagen deposition and pulmonary fibrosis (modified Ascroft scale) [33] was shown in Fig. 4c and d, respectively. These observations suggested that CLEC5A and TLR2 play critical roles in SARS-CoV-2-induced lung fibrosis. The quantitation of collagen area in lung was shown in Fig. 4b. Thus, we concluded that SARS-CoV-2 activated CLEC5A and TLR2 to induce lung inflammatory reactions, thrombosis, and collagen deposition, and PLT-EVs further enhanced NET formation via CLEC5A. These observations further suggested that EVs from virus-activated platelets are potent endogenous danger signals to enhance inflammatory reactions in vivo.

Discussion

It has been shown that lung is responsible for 50% of platelet biogenesis or 10 million platelets per hour [35]. Moreover, platelets were hyperactivated in clinically ill COVID-19 patients [13, 14], and contributed to coagulopathy in COVID-19 patients [18]. Thus, we are interested to understand the mechanism of platelet-mediated immunothrombosis in SARS-CoV-2 infection. In this study, we demonstrated that platelets enhanced SARS-CoV-2-induced NET formation (Additional file 1: Fig. S1). Moreover, SARS-CoV-2/platelets-induced NETs were detached from the coverslip and floated in the culture medium at 20 h post-incubation, resulting in less NETs attached to coverslip [Additional file 1: Fig. S2a (lower panel) and S2b (# above white column)]. This phenomenon was not observed in DV/platelets-induced NET formation, suggesting the aggregated floating NETs may contribute to microemboli in COVID-19 patients. Furthermore, SARS-CoV-2 and COVID-19 EVs induced NET formation via CLEC5A and TLR2, and *clec5a*$^{-/-}$*tlr2*$^{-/-}$ mice were resistant to SARS-CoV-2-induced lung inflammation and collagen deposition. These observations suggest that platelets contribute to SARS-CoV-2-induced inflammation significantly, and blockade of CLEC5A and TLR2 may be beneficial to alleviate thromboinflammation and reduce intravascular coagulopathy in COVID-19 patients.

It has been shown that serum EV level correlates with disease severity in COVID-19 patients [36, 37]. Moreover, Syk inhibitor R406 was shown to prevent NETosis of healthy donor neutrophils stimulated with COVID-19 patient plasma [38]. In this study, we further demonstrated that COVID-19 EVs express abundant markers of

(See figure on next page.)

Fig. 3 Attenuation of SARS-CoV-2-induced thromboinflammation in CLEC5A and TLR2 deficient mice. C57BL/6 mice (WT) and *clec5a*$^{-/-}$*tlr2*$^{-/-}$ mice were inoculated with AAV-hACE2 for 14 days, followed by intranasal inoculation of SARS-CoV-2 (8×10^4 PFU/per mice). Tissues were collected at 3 days and 5 days post-infection. $N = 3$ of each group **a** The level of proinflammatory cytokines and chemokines were measured by real-time PCR and presented as fold change (compared to AAV-hACE2 uninfected mice/mock). **b**–**d** NET structure and thrombus were detected by Hoechst. 33342 (blue), anti-MPO antibody (green), anti-citrullinated histone H3 (red), anti-CD42b antibody (yellow) (**b**), and images were captured by a confocal microscope and subjected to determine the area of MPO (**c**) and CD42b (**d**) using MetaMorph™ software. **e** Cell infiltrated to lung at 3 d.p.i.. Interstitial macrophage (interstitial MΦ) was defined as $CD11b^+CD64^+F4/80^+$ cells; monocyte-derived dendritic cell (DC)/macrophage (MΦ) was defined as $CD11b^+CD64^+Ly6C^+$; $Ly6C^+$ monocyte was defined as $Ly6C^+$. The cell number of each cell population was calculated using the multiple fluorescent staining image and analyzed by software MetaMorph™, and the data was presented as cell number/ per 664225 (815 × 815). Scale bar is 200 μm. Data are represented as mean ± SEM. *$p < 0.05$, **$p < 0.01$, ***$p < 0.001$, **** $p < 0.0001$ (Student's *t*-test)

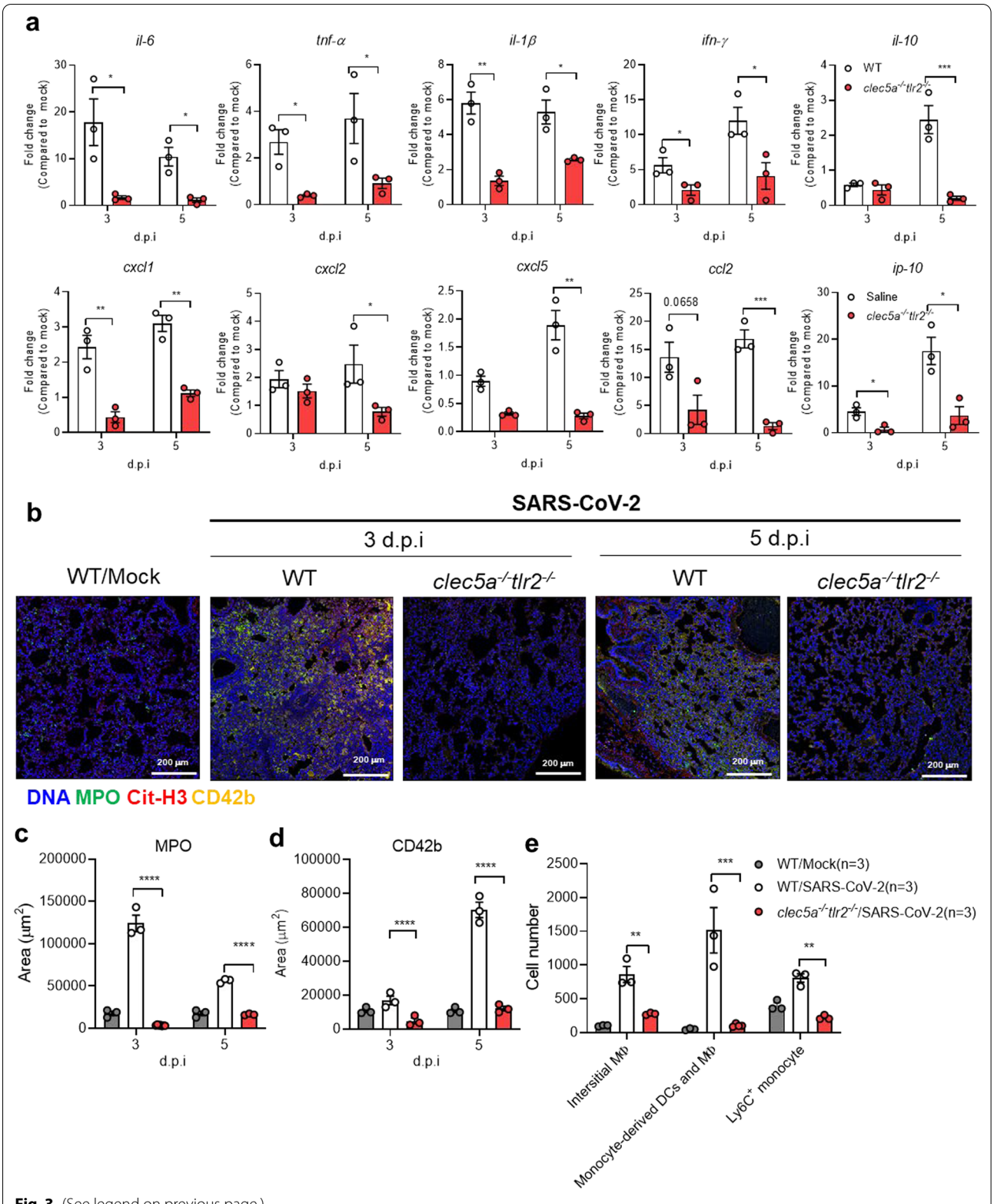

Fig. 3 (See legend on previous page.)

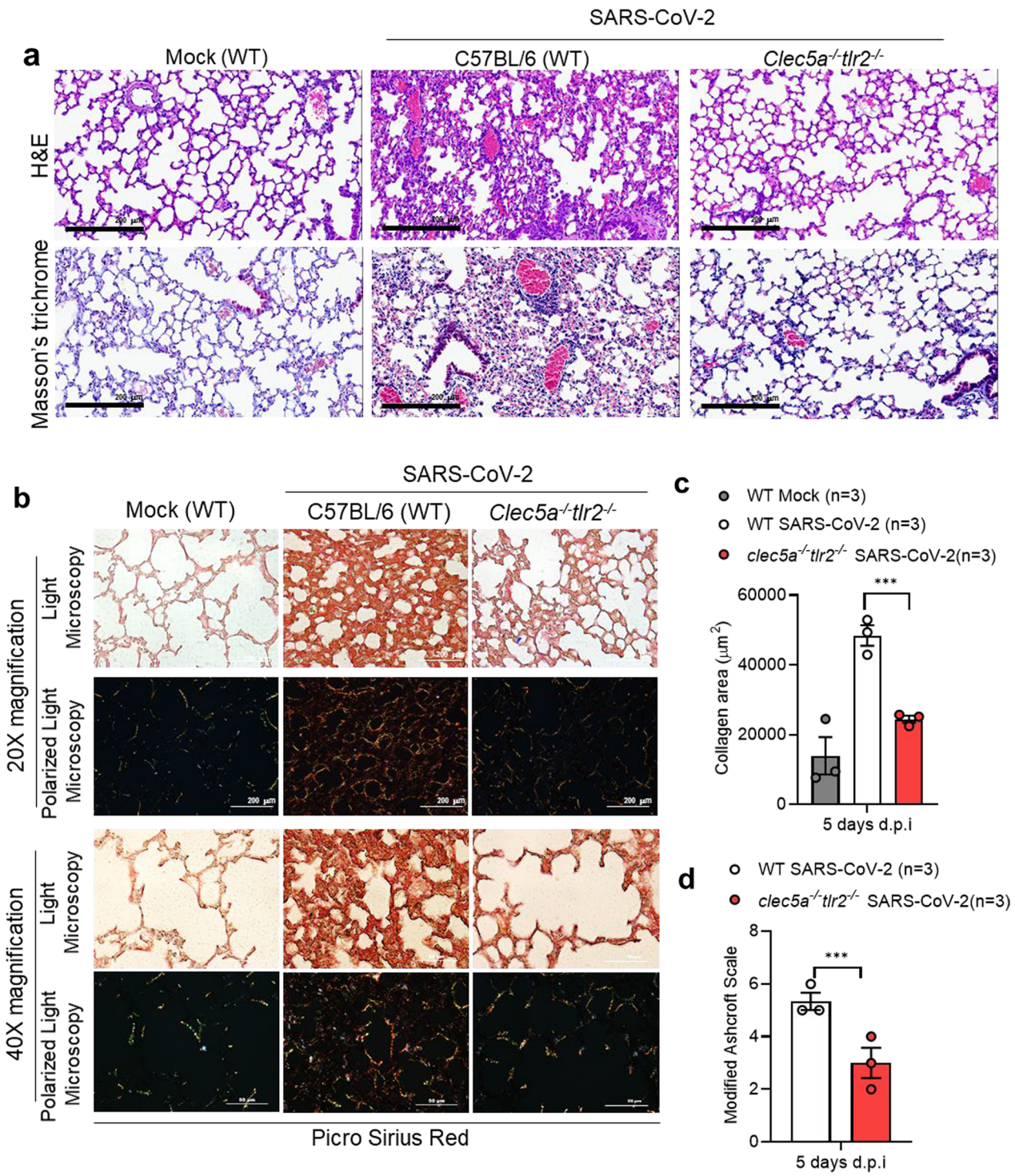

Fig. 4 CLEC5A and TLR2 are critical in SARS-CoV-2-induced collagen deposition SARS-CoV-2-challenged mice were sacrificed to harvest lung at 5 days post-infection. **a** Lung sections were stained with H&E and Masson's trichrome. 20× magnification. **b** Picro Sirius Red dye and captured the image under light microscopy (upper panel) and polarized light microscopy (lower panel) under 20× and 40× magnification. The scale bar is 200 μm in 20× magnification and 50 μm in 40× magnification. **c** The level of collagen deposition (Pico Sirius Red) was quantified using MetaMorph™ software and presented as area (μm^2). **d** The pulmonary fibrosis level was evaluated using Modified Ashcroft Scale. Data are mean ± SEM. ***$p < 0.001$ (Student's *t*-test). $N = 3$ of each group

activated platelets, enhance NET formation via CLEC5A and TLR2 (Fig. 3d). These observations are in accord with our previous report that DV activates platelets to release EVs, which are critical endogenous danger signals to trigger NET formation and inflammatory reactions via Syk-coupled CLEC5A and TLR2 [26, 27].

Recently, SARS-CoV-2 was shown to bind ACE2 in platelets to enhance NETosis [18]. However, mass spectrometry [39] and RNA-seq analyses [40, 41] did not detect ACE2 and TMPRSS2 in platelets and megakaryocytes. Increasing evidence indicates that lectins play critical roles in virus-induced systemic inflammation and NET formation [42]. C-type lectins (DC-SIGN and L-SIGN) and sialic acid-binding immunoglobulin-like lectin 1 (SIGLEC1) were shown to function as attachments receptors by enhancing ACE-2 mediated infection [43]. Furthermore, SARS-CoV-2 was reported to exacerbate inflammatory responses in myeloid cells through C-type lectin receptors and Tweety family members [44]. We have shown that DV was captured by DC-SIGN to activate the CLEC2 to release EVs from platelets [26]. Moreover, DV has been shown to be captured by C-type lectins heterocomplex (DC-SIGN and mannose receptor) to trigger inflammation and NETosis via CLEC5A and TLR2 [26, 27, 45]. Thus, it would be very interesting to test whether CLEC2/DC-SIGN complex is responsible for SARS-CoV-2-induced platelet activation in the future.

It has been reported that clinical symptoms, laboratory features and autopsy findings between dengue fever and COVID-19 are similar and are difficult to distinguish, and some patients who were initially diagnosed with dengue, but were later confirmed to have COVID-19 [46]. Moreover, autopsy of COVID-19 patients demonstrated that cells involved in the pathogenesis of COVID-19 and dengue are similar [47]. In this study, we found that platelets and platelet-derived EVs play critical roles in the pathogenesis of SARS-CoV-2. Unlike the thread shape of NET formation caused by DV, SARS-CoV-2-induced robust aggregated NET formation in the presence of platelets. Because the aggregated NETs may detach from SARS-CoV-2-induced thrombi and form micro-emboli in vivo, this observation can explain why intracoagulopathy was only found in COVID-19 patients, but not in DV-infected patients. Thus, inhibition of platelet activation may become a novel strategy to attenuate virus-induced lung inflammatory reactions in the future.

Conclusions

This work clearly demonstrates that PLT-EVs from COVID-19 patients can enhance thromboinflammation via CLEC5A and TLR2, and further shows that PLT-EVs from virus-activated act as endogenous danger signals to cause systemic inflammation. As serum levels of PLT-EVs strongly associated with severity of SARS-CoV-2 infection [19] and thromboemboli contribute to the morbidity of post-acute sequelae of COVID (PASC) [9], CLEC5A and TLR2 are promising therapeutic targets to attenuate thromboinflammation and reduce the risk of post-acute COVID-19 syndrome in the future.

Supplementary Information

The online version contains supplementary material available at https://doi.org/10.1186/s12929-022-00832-z.

Additional file 1: Figure S1. Platelet enhances SARS-CoV-2-induced NET formation. Human neutrophils (4×10^5/ml) were incubated with SARS-CoV-2 (MOI = 1) in the presence or absence of autologous platelets (4×10^6/ml) for 5 h at 37 °C. The NET structure was visualized by staining with DNA (blue), Cit-H3 (green), and MPO (red) then captured by confocal microscopy under 2000 × magnification. The colocalization of DNA, Cit-H3, and MPO was color in white. The scale bar is 10 μm. **Figure S2.** Platelet promotes severe NETs under SARS-CoV-2 stimulation after 20 h incubation. (a&b) Neutrophils (4×10^5/ml) from healthy volunteers were stimulated with SARS-CoV-2 (MOI = 0.1 or 1) with or without autologous platelets (4×10^6/ml) for 20 h at 37 ·C. Samples were fixed and stained with DNA (blue), Cit-H3 (green), and MPO (red). The image was captured by confocal microscopy under 400 × magnification (a). The scale bar is 10 μm. The level of NET was calculated using the image of Cit-H3 from 5 healthy donors (b). #: NET structure was detached from platelets and floated in culture supernatant. Data was presented as mean of area (μm^2) ± SEM. **** $p < 0.0001$ (Student's *t*-test). **Figure S3.** SARS-CoV-2-induced NETs and immunothrombosis are CLEC5A/TLR2-dependent. WT and *clec5a*$^{-/-}$*tlr2*$^{-/-}$ mice were inoculated with AAV-ACE2 at day 14 day before SARS-CoV-2 challenge, and lung samples were collected at day 3 and day 5 post-infection. Tissue sections were stained with Hoechst 33342 for DNA (blue), anti-MPO antibody (green), anti-Cit-H3 antibody (red), and anti-CD42b antibody (yellow) to visualize the structure of NETs and immunothrombosis. Scale bar is 100 μm.

Additional file 2: Table S1. Sequences of qPCR primers.

Acknowledgements

This work was supported by Academia Sinica (AS-IDR-110-01, AS-GC-110-MD01), and Biotechnology Research Park Translational Project (AS-BRPT-110-02). The other supports are from Academia Sinica Investigator Award (AS-IA-109-L02), Ministry of Science and Technology (MOST 107-2321-B-001-015), and VGH, TSGH, AS Joint Research Program (VTA110-V5-5-1). We are grateful to Dr. Yu-Chi Chou to provide SARS-CoV-2 spike pseudotyped virus, and Dr. Jia-Tsrong Jan for technical support.

Author contributions

PSS designed, performed, analyzed experiments, and wrote the manuscript. SPY, YCP, CPS performed experiments, MHT provided animal models, SLH designed, analyzed experiments, data interpretation, and drafted and revised the manuscript. All authors read and approved the final manuscript.

Funding

This work was supported by Academia Sinica (AS-IDR-110-01, AS-GC-110-MD01), and Biotechnology Research Park Translational Project (AS-BRPT-110-02). The other supports are from Academia Sinica Investigator Award (AS-IA-109-L02), Ministry of Science and Technology (MOST 107-2321-B-001-015), and VGH, TSGH, AS Joint Research Program (VTA110-V5-5-1). We are grateful to Dr. Yu-Chi Chou to provide SARS-CoV-2 spike pseudotyped virus, and Dr. Jia-Tsrong Jan for technical support.

Availability of data and materials

The datasets generated and/or analyzed in the current study are not publicly available due to patient privacy, however they are available from the corresponding author on reasonable request.

Declarations

Ethics approval and consent to participate

This study was conducted under the Helsinki Declaration of 1975. All patients provided written informed consent before enrollment, and the study was approved by the Research Ethics Committee of Academia Sinica, Taipei (AS-IRB01-20024, AS-IRB01-20025). Statement of animal operation in BSL-3 biosafety animal facility: All mouse works were conducted in accordance with the "Guideline for the Care and Use of Laboratory Animals" as defined by the Council of Agriculture, Taiwan. Mouse work was approved by the Institutional Animal Care and Use Committee of Academia Sinica (protocol ID: 20-05-1471 and 19-07-1330). The Institutional Biosafety Committee of Academia Sinica approved work with infectious SARS-CoV-2 virus strains under BSL3 conditions. All sample processes were conducted according to "Interim Laboratory Biosafety Guidelines for Handling and Processing Specimens Associated with Coronavirus Disease 2019 (COVID-19)" recommended by CDC.

Consent for publication

Not applicable.

Competing interests

The authors declare that they have no competing interests.

Author details

[1]Genomics Research Center, Academia Sinica, 128 Academia Road, Sec. 2, Nankang, Taipei 115, Taiwan. [2]Institute of Biomedical Sciences, Academia Sinica, Taipei, Taiwan. [3]Institute of Clinical Medicine, National Yang Ming Chiao Tung University, Taipei, Taiwan. [4]Department of Medical Research, Taipei Veterans General Hospital, Taipei, Taiwan. [5]Graduate Institute of Cancer Biology and Drug Discovery, Taipei Medical University, Taipei, Taiwan.

Received: 6 April 2022 Accepted: 27 June 2022
Published online: 11 July 2022

References

1. https://www.who.int/emergencies/diseases/novel-coronavirus-2019/technical-guidance/naming-the-coronavirus-disease-(covid-2019)-and-the-virus-that-causes-it.
2. Zhu N, et al. A novel coronavirus from patients with pneumonia in China, 2019. N Engl J Med. 2020;382(8):727–33.
3. Huang C, et al. Clinical features of patients infected with 2019 novel coronavirus in Wuhan, China. Lancet. 2020;395(10223):497–506.
4. Zhou F, et al. Clinical course and risk factors for mortality of adult inpatients with COVID-19 in Wuhan, China: a retrospective cohort study. Lancet. 2020;395(10229):1054–62.
5. Klok FA, et al. Incidence of thrombotic complications in critically ill ICU patients with COVID-19. Thromb Res. 2020;191:145–7.
6. Oxley TJ, et al. Large-vessel stroke as a presenting feature of COVID-19 in the young. N Engl J Med. 2020;382(20): e60.
7. Wichmann D, et al. Autopsy findings and venous thromboembolism in patients with COVID-19. Ann Intern Med. 2020.
8. Lax SF, et al. Pulmonary arterial thrombosis in COVID-19 with fatal outcome: results from a prospective, single-center, clinicopathologic case series. Ann Intern Med. 2020.
9. Gu SX, et al. Thrombocytopathy and endotheliopathy: crucial contributors to COVID-19 thromboinflammation. Nat Rev Cardiol. 2021;18(3):194–209.
10. Martinod K, Wagner DD. Thrombosis: tangled up in NETs. Blood. 2014;123(18):2768–76.
11. Ng H, et al. Circulating markers of neutrophil extracellular traps are of prognostic value in patients with COVID-19. Arterioscler Thromb Vasc Biol. 2021;41(2):988–94.
12. Barnes BJ, et al. Targeting potential drivers of COVID-19: Neutrophil extracellular traps. J Exp Med. 2020; 217(6).
13. Yatim N, et al. Platelet activation in critically ill COVID-19 patients. Ann Intensive Care. 2021;11(1):113.
14. Zaid Y, et al. Platelets can associate with SARS-Cov-2 RNA and are hyperactivated in COVID-19. Circ Res. 2020.
15. Middleton EA, et al. Neutrophil extracellular traps contribute to immunothrombosis in COVID-19 acute respiratory distress syndrome. Blood. 2020;136(10):1169–79.
16. Bonaventura A, et al. Endothelial dysfunction and immunothrombosis as key pathogenic mechanisms in COVID-19. Nat Rev Immunol. 2021;21(5):319–29.
17. Bautista-Becerril B, et al. Immunothrombosis in COVID-19: implications of neutrophil extracellular traps. Biomolecules. 2021; 11(5).
18. Zhang S, et al. SARS-CoV-2 binds platelet ACE2 to enhance thrombosis in COVID-19. J Hematol Oncol. 2020;13(1):120.
19. Cappellano G, et al. Circulating platelet-derived extracellular vesicles are a hallmark of sars-cov-2 infection. Cells. 2021; 10(1).
20. Zuo Y, et al. Neutrophil extracellular traps in COVID-19. JCI Insight. 2020.
21. Chen ST, et al. CLEC5A is critical for dengue-virus-induced lethal disease. Nature. 2008;453(7195):672–6.
22. Wu MF, et al. CLEC5A is critical for dengue virus-induced inflammasome activation in human macrophages. Blood. 2013;121(1):95–106.
23. Huang YL, et al. CLEC5A is critical for dengue virus-induced osteoclast activation and bone homeostasis. J Mol Med (Berl). 2016;94(9):1025–37.
24. Sung PS, Chang WC, Hsieh SL. CLEC5A: a promiscuous pattern recognition receptor to microbes and beyond. Adv Exp Med Biol. 2020;1204:57–73.
25. Chen ST, et al. CLEC5A is a critical receptor in innate immunity against Listeria infection. Nat Commun. 2017;8(1):299.
26. Sung PS, Huang TF, Hsieh SL. Extracellular vesicles from CLEC2-activated platelets enhance dengue virus-induced lethality via CLEC5A/TLR2. Nat Commun. 2019;10(1):2402.
27. Sung PS, Hsieh SL. CLEC2 and CLEC5A: pathogenic host factors in acute viral infections. Front Immunol. 2019;10:2867.
28. Youn YJ, et al. Nucleocapsid and spike proteins of SARS-CoV-2 drive neutrophil extracellular trap formation. Immune Netw. 2021;21(2): e16.
29. Zheng M, et al. TLR2 senses the SARS-CoV-2 envelope protein to produce inflammatory cytokines. Nat Immunol. 2021;22(7):829–38.
30. Khan S, et al. SARS-CoV-2 spike protein induces inflammation via TLR2-dependent activation of the NF-kappaB pathway. bioRxiv. 2021.
31. Glowacka I, et al. Evidence that TMPRSS2 activates the severe acute respiratory syndrome coronavirus spike protein for membrane fusion and reduces viral control by the humoral immune response. J Virol. 2011;85(9):4122–34.
32. Sun CP, et al. Rapid generation of mouse model for emerging infectious disease with the case of severe COVID-19. PLoS Pathog. 2021;17(8): e1009758.
33. Hubner RH, et al. Standardized quantification of pulmonary fibrosis in histological samples. Biotechniques. 2008;44(4):507–11, 514–7.
34. George PM, Wells AU, Jenkins RG. Pulmonary fibrosis and COVID-19: the potential role for antifibrotic therapy. Lancet Respir Med. 2020;8(8):807–15.
35. Lefrancais E, et al. The lung is a site of platelet biogenesis and a reservoir for haematopoietic progenitors. Nature. 2017;544(7648):105–9.
36. Rosell A, et al. Patients with COVID-19 have elevated levels of circulating extracellular vesicle tissue factor activity that is associated with severity and mortality-brief report. Arterioscler Thromb Vasc Biol. 2021;41(2):878–82.
37. Hassanpour M, et al. The role of extracellular vesicles in COVID-19 virus infection. Infect Genet Evol. 2020;85: 104422.
38. Strich JR, et al. Fostamatinib inhibits neutrophils extracellular traps induced by COVID-19 patient plasma: a potential therapeutic. J Infect Dis. 2021;223(6):981–4.
39. Burkhart JM, et al. The first comprehensive and quantitative analysis of human platelet protein composition allows the comparative analysis of structural and functional pathways. Blood. 2012;120(15):e73-82.
40. Rowley JW, et al. Genome-wide RNA-seq analysis of human and mouse platelet transcriptomes. Blood. 2011;118(14):e101–11.
41. Machlus KR, et al. Synthesis and dephosphorylation of MARCKS in the late stages of megakaryocyte maturation drive proplatelet formation. Blood. 2016;127(11):1468–80.
42. Sung PS, Hsieh SL. C-type lectins and extracellular vesicles in virus-induced NETosis. J Biomed Sci. 2021;28(1):46.
43. Lempp FA, et al. Lectins enhance SARS-CoV-2 infection and influence neutralizing antibodies. Nature. 2021;598(7880):342–7.

44. Lu Q, et al. SARS-CoV-2 exacerbates proinflammatory responses in myeloid cells through C-type lectin receptors and Tweety family member 2. Immunity. 2021;54(6):1304-1319 e9.
45. Lo YL, et al. Dengue virus infection is through a cooperative interaction between a mannose receptor and CLEC5A on macrophage as a multivalent hetero-complex. PLoS ONE. 2016;11(11): e0166474.
46. Yan G, et al. Covert COVID-19 and false-positive dengue serology in Singapore. Lancet Infect Dis. 2020;20(5):536.
47. Rapkiewicz AV, et al. Megakaryocytes and platelet-fibrin thrombi characterize multi-organ thrombosis at autopsy in COVID-19: a case series. EClinicalMedicine. 2020;24: 100434.

Publisher's Note